BASIC SCIENCE

Nanomedicine: Nanotechnology, Biology, and Medicine
11 (2015) 479–487

Original Article

nanomedjournal.com

In vivo biodistribution and clearance of peptide amphiphile micelles

Eun Ji Chung, PhD[a], Laurie B. Mlinar, BS[b], Matthew J. Sugimoto, BS[a], Kathryn Nord, BS[a], Brian B. Roman, PhD[c], Matthew Tirrell, PhD[a,*]

[a]*Institute for Molecular Engineering, University of Chicago, Chicago, IL, USA*
[b]*Dept. of Chemical and Biomolecular Engineering, University of California, Berkeley, Berkeley, CA, USA*
[c]*Dept. of Radiology, University of Chicago, Chicago, IL, USA*

Received 19 March 2014; revised 13 August 2014; accepted 22 August 2014

Abstract

Peptide amphiphiles (PAs) are promising biomaterials for medical applications. To translate the use of PAs successfully from laboratories to clinics, *in vivo* studies regarding the safety of these nanomaterials are required. To examine the toxicity and clearance of PA biomaterials, we intravenously administered cy7-labeled, spherical PA micelles, control micelles without a peptide sequence, or PBS in a murine model and investigated biocompatibility, biodistribution, and clearance. Both peptide and non-peptide labeled micelles were approximately 8 nm in diameter, but of opposite surface charge. Neither micelle type caused aggregation or hemolysis of red blood cells. All micelles primarily accumulated in the bladder and were present in urine samples confirming elimination through renal clearance. *Ex vivo* imaging showed that micelles were also found in the liver suggesting some involvement of the reticuloendothelial system. However, no evidence of toxicity was found within the liver, spleen, kidney, bladder, intestines, lung, and heart.

From the Clinical Editor: Safety studies related to peptide amphiphile biomaterials are discussed in this paper, demonstrating that organotoxicity is unlikely with these materials, however, RES activation in the liver may be of consideration in further studies and needed for potential applications.

Key words: Peptide amphiphile; Micelle; Nanoparticle; Biodistribution; Clearance

Recent developments in nanoscale engineering and molecular design are advancing the field of biomaterials toward bioactive, multifunctional, and targeting materials for applications in tissue engineering, drug delivery, and imaging.[1–4] Specifically, peptide-based nanomaterials have gained considerable interest due to the design flexibility and structural diversity that they provide.[5–8] Furthermore, the use of peptides provides a strategy to incorporate a biological signal for tissue-specific binding and localization, as well as enhancing the potential for biocompatibility and biodegradation.[6,9] An example of such design is peptide amphiphile (PA) biomaterials, a growing class of molecules that contain a biologically active peptide "head group" and a hydrophobic alkyl "tail."[10,11] Under aqueous conditions, PAs can self-assemble into well-defined spherical micelles in which the hydrophobic tails aggregate in the core and the peptides are presented on the exterior. The concentrated, multivalent display of peptides and the ability to incorporate multifunctionality through the mixing of several amphiphile monomers are characteristics that are especially favorable for targeting diseased tissues for therapeutic and diagnostic applications in medicine.[1,12] Furthermore, with different molecular architectures, PAs assemble into extended, fiber-like micelles that have proven useful for tissue engineering and regenerative medicine.[13]

In our earlier studies, fluorescently-labeled spherical micelles containing the fibrin-binding peptide cysteine–arginine–glutamic acid–lysine–alanine (CREKA) were reported to home to sites of atherosclerotic plaques upon intravenous injection in the ApoE knock-out mouse model.[1] Furthermore the potential to deliver a therapeutic peptide was demonstrated. When properly designed, many nanomaterials, including micelles, have been proposed as therapeutic carriers for their ability to deliver drugs in the optimum dosage range which results in improved intracellular penetration and therapeutic efficacy, enhanced absorption into selected tissues, and reduced toxic, side effects.[14] Today, paclitaxel and doxorubicin are two examples of chemotherapeutic agents that have been encapsulated into polymeric nanomaterials and are currently used in clinical practice.[15–17]

The authors would like to acknowledge the support from the American Heart Association Postdoctoral Fellowship granted to E. Chung and the government support awarded by the DoD, AFOSR, National Defense Science and Engineering Graduate (NDSEG) Fellowship, 32 CFR 168a, granted to L. Mlinar that supported this research. There are no conflicts of interests.

*Corresponding author at: Institute for Molecular Engineering, University of Chicago, Chicago, IL, USA.
E-mail address: mtirrell@uchicago.edu (M. Tirrell).

http://dx.doi.org/10.1016/j.nano.2014.08.006
1549-9634/

The physiochemical characteristics including particle size, surface charge, and shape have been known to influence the clearance and *in vivo* biodistribution of a nanomaterial.[18–20] In general, smaller, spherical nanoparticles (3-6 nm) are less likely to be taken up by macrophages than larger ones since the highly curved surfaces do not allow for easy complement activation.[21–24] Small particles are distributed widely in a variety of organs by crossing tight endothelial junctions and are often excreted through the renal system.[18] Larger particles (>10 nm), on the other hand, are rapidly cleared by the reticuloendothelial system (RES), specifically through sequestration by sinusoids in the spleen and fenestra of the liver.[19,24] Furthermore, elimination of molecules within the intermediate range, 6-8 nm, depends upon both size and charge of the particle.[21] In general, while positively-charged nanoparticles have been reported to be readily taken up by macrophages and clearance facilitated by RES due to the interaction with the negatively-charged cell membrane, other researchers demonstrate anionic nanoparticles to enhance uptake through RES by binding to cationic sites on the macrophage surface.[25,26] Still, others report neutralizing the nanoparticle surface through the addition of polyethylene glycol (PEG) to circumvent the adsorption of serum proteins characteristic to either charged species, which can increase the hydrodynamic, *in vivo* diameter, and ultimately lead to clearance via RES.[18]

In addition to size and surface charge, the shape of the nanomaterial can also play a role in determining its pharmacokinetic property and biodistribution.[27] For example, in comparison to its spherical counterpart, gold nanorods were taken up by macrophages and accumulated in the liver to a lesser degree.[28] Given the unique set of properties to each nanoparticle system and recognizing that no universal rules exist that can be applied to predict the *in vivo* behavior of all nanoparticles, it is imperative that the safety of the nanomaterials be evaluated on an individual basis. In addition to understanding biocompatibility and clearance, physiochemical design of the nanomaterial can be further considered and tailored for future applications *in vivo*.

To this end, in this study, we investigate the biodistribution and clearance of spherical micelles composed of CREKA PAs in the ApoE knock-out mouse, a murine atherosclerosis model. Despite increasing interest and use, there are very limited studies available for exploring the biocompatibility and tissue distribution of nanomaterials based on PAs. Even more scarce are studies conducted in disease models in which most nanocarriers are studied and essential organs such as the liver are already compromised and can be further aggravated by nanoparticles.[29–31] In the present study, we injected PA micelles with varying cy7 fluorescence with or without the peptide, CREKA, to delineate the safety of PA micelles in a disease model. Cy7 was chosen for the fluorophore to be incorporated into micelles because its excitation and emission wavelength in the deep red range is optimal to achieve both good tissue penetration and low autofluorescence.[32] To our knowledge, this is the first study to evaluate PAs for their *in vivo* biodistribution, clearance, and organ toxicity.

Methods

Micelle synthesis

CREKA and non-targeting (NT) micelles were synthesized and assembled as previously described.[33] Briefly, the [Cys-Arg-Glu-Lys-Ala] peptide was synthesized using standard Fmoc-mediated solid phase peptide synthesis methods on rink amide resin (Anaspec, Fremont, CA) using an automated PS3 Benchtop Peptide Synthesizer (Protein Technologies, Tucson, AZ). The N-terminus was acetylated using 10× molar excess of acetic anhydride in DMF. Peptides were cleaved and deprotected with 94:2.5:2.5:1 by volume trifluoroacetic acid: 1,2-ethanedithiol: H2O:triisopropylsilane and were precipitated and washed several times with cold diethyl ether, dissolved in water, lyophilized, and stored as lyophilized powders at −20 °C. Crude peptide mixtures were purified by reverse-phase HPLC (Prominence, Shimadzu, Columbia, MD, USA) on a C8 column (Waters, Milford, MA, USA) at 55 °C using 0.1% trifluoroacetic acid in acetonitrile/water mixtures and characterized by MALDI-TOF mass spectral analysis (Biflex III, Bruker, Billerica, MA, USA). Cysteine-containing peptides were conjugated via a thioether linkage to 1,2-distearoyl-*sn*-glycero-3-phosphoethanolamine-*N*-[maleimide(polyethylene glycol)-2000], or DSPE-PEG(2000)-maleimide (Avanti Polar Lipids, Alabaster, AL, USA) by adding a 10% molar excess of the peptide to lipid in water. After reaction at room temperature for 24 h, the resulting product was purified on a C4 column and characterized as described above. Cy7 was conjugated via an amide bond to DSPE-PEG(2000)-amine (Avanti Polar Lipids, Alabaster, AL, USA) by adding an equal molar equivalent of cy7 mono-*N*-hydroxysuccinimide ester (GE Healthcare Life Sciences, Pittsburgh, PA, USA) to the lipid dissolved in 10 mM aqueous sodium carbonate buffer (pH 8.5). After reaction at room temperature for 24 h, the mixture was also purified on a C4 column and characterized as described above.

CREKA micelles were assembled by dissolving the cy7 and peptide-containing DSPE-PEG(2000) amphiphiles (2.5:97.5, 5:95, 10:90, or 25:75 molar ratio) in methanol, mixing the components, and evaporating the mixed solution under nitrogen. The resulting film was dried under vacuum over night, and then hydrated at 80 °C for 30 min in water or PBS and allowed to cool to room temperature. Non-targeting (NT) micelles were assembled by combing DSPE-PEG(2000)-cy7 and DSPE-PEG (2000)-maleimide using the molar ratios specified above.

Micelle characterization

Dynamic light scattering (DLS)

Stock solutions of 100 μM DSPE-PEG(2000)-CREKA or DSPE-PEG(2000)-maleimide in water were used to confirm the presence of small spheroidal micelles. DLS measurements were determined at 90° and 637 nm using a Brookhaven Instruments (Holtzville, NY, USA) system consisting of a BI-200SM goniometer and a BI-9000AT autocorrelator. In order to measure the change in micelle size due to protein adsorption, 100 μM DSPE-PEG(2000)-CREKA or DSPE-PEG(2000)-maleimide in Dulbecco's Modified Eagle's Medium (DMEM) supplemented with 10% fetal bovine serum (FBS, Life Technologies, Grand

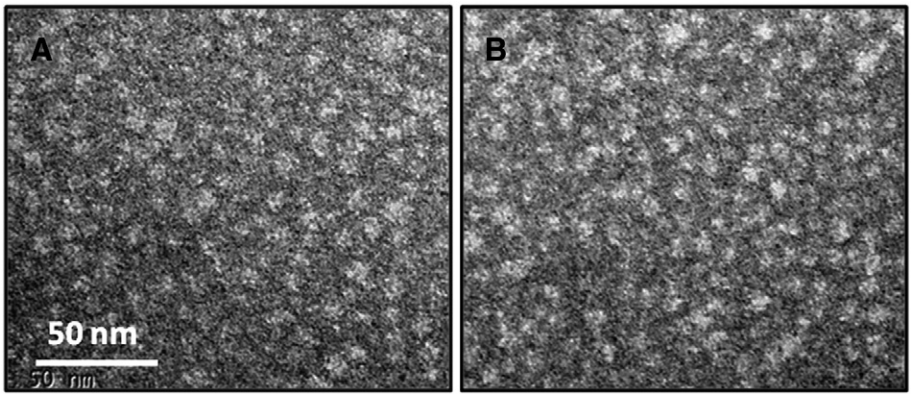

Figure 1. Transmission electron micrograph of (**A**) NT and (**B**) CREKA micelles.

Island, NY, USA) was incubated at 37 °C for 2 h before measurements were conducted.

Transmission electron microscopy (TEM)

Negatively stained samples for TEM were prepared by layering the 100 μM DSPE-PEG(2000)-CREKA or DSPE-PEG(2000)-maleimide solution on 400 mesh lacey carbon grids (Ted Pella, Redding, CA) for 2 min. Excess liquid was wicked away with filter paper and the grid was washed with Milli-Q water before placing 1 wt.% uranyl acetate solution for 2 min and washing with Milli-Q water. Dried samples were imaged on a JEOL 1230 TEM, immediately (JEOL, Ltd., Tokyo, Japan).

Zeta potential

Zeta potential of 100 μM DSPE-PEG(2000)-CREKA or DSPE-PEG(2000)-maleimide dissolved in water was measured (Zetasizer Nano ZS, Malvern, Worcestershire, United Kingdom, N = 3).

Critical micelle concentration determination via 1,6-diphenyl-1,3,5-hexatriene (DPH) fluorescence

The critical micelle concentration (CMC) was determined using DPH fluorescence.[34] This method relies on an increase in DPH fluorescence as it partitions from aqueous solution into the hydrophobic micelle core. Solutions of DSPE-PEG(2000)-CREKA or DSPE-PEG(2000)-maleimide ranged in concentrations from 316 to 0.178 μM. DPH was dissolved in tetrahydrofuran (THF) and a small amount of this solution was added to each solution to achieve 1 μM DPH with a residual THF volume percentage of approximately 0.1. Solutions containing PA and DPH were allowed to equilibrate for 1 h prior to measurement using a Tecan Infinite 200 plate reader (Mannedorf, Switzerland). DPH was excited at 350 nm and fluorescence emission was measured at 428 nm.

Erythrocyte aggregation

The erythrocyte aggregation test was performed using a simple slide test as previously reported.[35] Whole blood was drawn from female, 6 months old, transgenic mice homozygous for the *Apoe*^{tm1Unc} mutation (The Jackson Laboratory, Bar Harbor, ME, USA) via an open chest cardiac puncture and collected in tubes containing sodium citrate. Blood was centrifuged at 500 ×*g* at 4 °C for 10 min to separate erythrocytes from platelet-rich plasma. Erythrocytes were repeatedly washed with PBS by centrifugation and were resuspended at 0.5% (vol/vol) in PBS. Micelles were added to make a final concentration of 100 μM DSPE-PEG(2000)-CREKA or DSPE-PEG(2000)-maleimide (N = 3). After one hour, one drop of solution was trickled onto a slide inclined at an angle of 30° and allowed to run down by gravity, leaving a fine film. The slides were left to dry in that position at room temperature and imaged via light microscopy (Leica, DMI6000B, Buffalo Grove, IL). Representative images are presented.

Animal experiments

Female, 4 weeks old, transgenic mice homozygous for the *Apoe*^{tm1Unc} mutation (The Jackson Laboratory, Bar Harbor, ME, USA) were fed a high-fat diet that consists of 21% (wt/wt) fat, 0.15% (wt/wt) cholesterol, 19.5% (wt/wt) casein, and no sodium cholate (Harlan, Indianapolis, Indiana, USA) for 22 weeks to generate stage V lesions.[36] Wild-type (WT), background C57BL/6 mice were used as a control (The Jackson Laboratory, Bar Harbor, ME, USA). Mice were shaved and naired, and tail veins were dilated and sterilized with 70% ethanol before 100 μL of 1 mM or 10 mM DSPE-PEG(2000)-cy7:DSPE-PEG (2000)-CREKA or DSPE-PEG(2000)-cy7:DSPE-PEG(2000)-maleimide (2.5:97.5, 5:95, 10:90, or 25:75 molar ratio) suspended in PBS, or PBS alone was intravenously injected (N ≥ 3). Micelles were allowed to circulate for 24 h or 7 days before mice were anesthetized with 2.5% isoflurane in O_2 and whole body fluorescence imaging was conducted (IVIS 200, Xenogen, Caliper Life Sciences, Hopkinton, MA, USA). Mice were then euthanized via CO_2 overdose and the heart, lung, liver, spleen, intestines, kidney, and bladder harvested for toxicity and histological analysis. Near infrared fluorescence imaging of organs was conducted using an IVIS 200 and quantification of the fluorescence signal was achieved via the Living Image software (Perkin Elmer, Downers Grove, IL, USA). Urine samples were collected directly from the bladder, diluted 25× in PBS, and cy7 intensity quantified on a 96-well plate (ex. 746 nm, em. 776 nm, Infinite 200 Pro, Tecan Group Ltd.,

Table 1
DLS and zeta potential measurements of NT and CREKA micelles.

	Non-Targeting (NT) Micelles	CREKA Micelles
Diameter (nm)	7.8 ± 1.3	7.9 ± 1.1
ZP (mV)	−22.5 ± 5.2	36.3 ± 2.3

Mannedorf, Switzerland) to assess clearance through the renal system. All animal procedures followed NIH guidelines for the care and use of laboratory animals and were approved by the University of Chicago's Institutional Animal Care and Use Committee (Chicago, IL, USA).

Liver and spleen function

To assess liver function, an equal mass of tissue was homogenized in lysis buffer and liver levels of alanine aminotransferase (ALT) and aspartate aminotransferase (AST) were measured using commercial assay kits (Sigma Aldrich, St. Louis, MO, USA). In addition, the level of apoptosis in the liver and spleen was determined by colorimetric quantification of caspase-3 activity (R&D Systems, Minneapolis, MN, USA).

Histology

Following optical imaging and euthanasia, the heart, lung, intestines, liver, kidney, spleen, and bladder were fixed with 4% paraformaldehyde overnight at 4 °C. Tissue was then submerged in a 30% sucrose solution for 8 h and frozen in OCT (Tissue Tek, Sakura Finetek, Torrance, CA, USA) before 5-7 μm samples were cryosectioned (Microm HM 525, Fisher Scientific, Pittsburgh, PA, USA), stained with Hemotoxylin and Eosin (H and E), and imaged (DMI6000 B, Leica Microsystems, Inc., Buffalo Grove, IL, USA). Representative images are presented.

Statistical analysis

Data are expressed as mean ± SEM. A Student's *t* test was used to compare means of pairs and analysis of variance (ANOVA) using Newman–Keuls multiple comparison test post-hoc analysis was used to determine significant differences among three or more means. A *P* value of 0.05 or less was considered to be significant.

Results

Synthesis and characterization of micelles

The cysteine of the fibrin-binding peptide, CREKA, was conjugated to DSPE-PEG(2000)-maleimide via a thioether linkage and the resulting PAs self-assembled under aqueous conditions into spherical micelles with a diameter of 7.9 nm, confirmed via TEM and DLS (Figure 1 and Table 1). Control, non-targeting (NT) micelles without a peptide sequence were similar in size (7.8 nm) to CREKA micelles (Figure 1, Table 1), but varied in zeta potential measurements; the addition of the CREKA peptide increased the surface charge of micelles from −22.5 to 36.3 mV (Table 1).

As NT and CREKA micelles will be applied for biomedical applications that require intravenous injection, *in vitro* cytotoxicity of micelles on red blood cells was evaluated by erythrocyte aggregation assays (Supplementary Figure 1). Despite the differences in charge, both NT and CREKA micelles did not cause erythrocyte aggregation compared to PBS-treated controls, and no sign of hemolysis was observed at 1 h post-incubation.

Biodistribution and clearance of micelles

In order to ensure that the biodistribution of micelles could be fully ascertained and imaged, the molar % of DSPE-PEG(2000)-cy7 incorporated into CREKA and NT micelles ranged from 2.5 to 25% for *in vivo* studies. NT or CREKA micelles with 2.5, 5, 10, or 25 molar % of DSPE-PEG(2000)-cy7 were intravenously injected through the tail vein of ApoE knock-out mice. As the critical micelle concentration (CMC) of NT and CREKA amphiphiles was determined to be approximately 2.2 and 3.3 μM using the DPH fluorescence assay (Supplementary Figure 2), the concentration and volume of micelles injected *in vivo* were such that it remained above the CMC even upon injection into the total blood volume in circulation.[1,37] After 24 h in blood circulation, *in vivo* imaging confirmed NT and CREKA micelles to predominantly accumulate in the bladder, most evident in mice injected with micelles containing 25 molar % DSPE-PEG(2000)-cy7 (Figure 2, *A*). To further confirm elimination of micelles through renal clearance, urine was collected directly from the bladder and fluorescence measured (Figure 2, *B*). An increase in cy7 intensity correlated with increasing cy7 composition of the micelle (NT 2.5: 45.8 ±17.7, NT 5: 127.8 ± 26.0, NT 10: 172.2 ± 13.7, NT 25: 305.6 ±21.8, CREKA 2.5: 77.8 ± 8.3, CREKA 5: 94.4 ± 5.9, CREKA 10: 150 ± 25.8, CREKA 25: 345.8 ± 27.0, PBS: 36.1 ± 8.3). No statistical significance was found between NT vs. CREKA micelles with the same cy7 composition. When compared to PBS, statistical significance was found for all micelles except those with 2.5% cy7 content.

Figure 3 shows the distribution of micelles in ApoE knock-out mice containing 25 mol % cy7 within the heart, lung, liver, spleen, intestines, and kidney using optical imaging after 24 h. In addition to clearance through the renal system, NT and CREKA micelles were found to be primarily localized in the liver and kidney. Clearance and biodistribution of NT and CREKA micelles in wild-type (WT), background C57BL/6 mice were found to be similar to those of ApoE knock-out mice after 24 h in circulation (Supplementary Figure 3). After 7 days, over 90% of both NT and CREKA micelles were cleared from WT and ApoE knock-out mice, with residual micelles remaining in the liver and kidney (Supplementary Figures 3 and 4).

To evaluate the behavior of micelles at a higher dose, ApoE knock-out mice were treated with micelles containing 25 mol % cy7 at a concentration of 10 mM. All mice survived and after 24 h, NT and CREKA micelles accumulated in the bladder as well as in the liver, similar to mice treated with micelles at a concentration of 1 mM (Supplementary Figures 5 and 6). Supplementary Figure 6 shows the biodistribution of 10 mM NT and CREKA micelles; in addition to the bladder and liver,

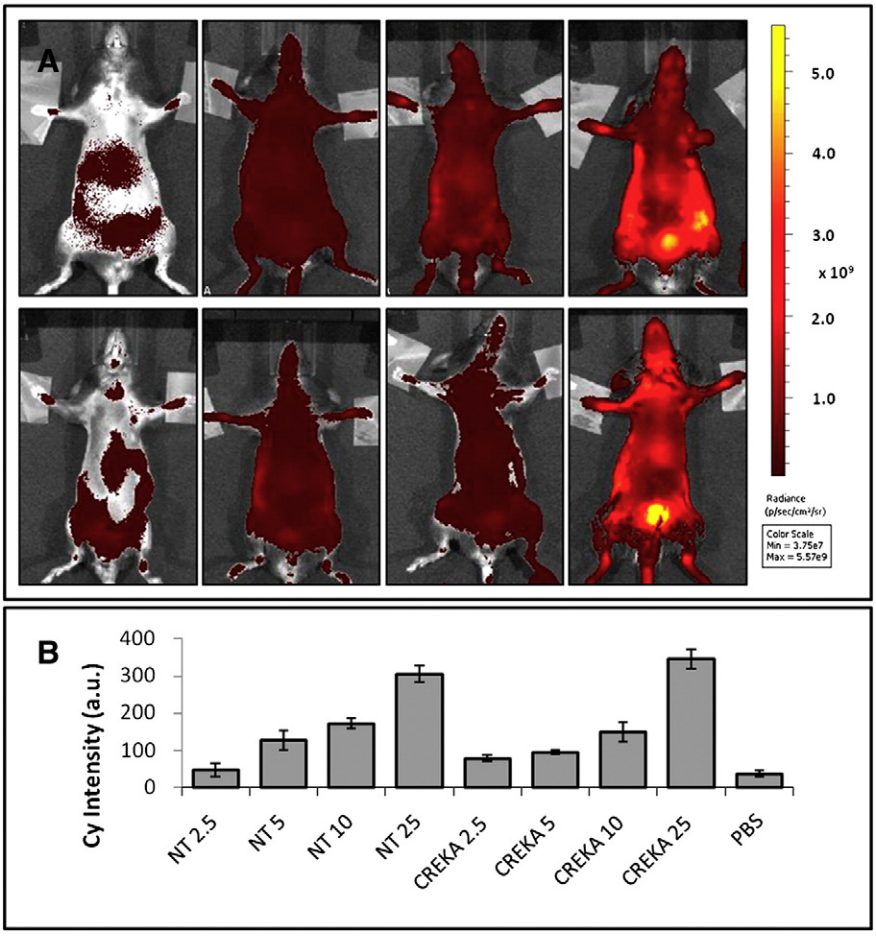

Figure 2. Micelles are excreted through the bladder after 24 h. (**A**) In vivo, optical images of ApoE knock-out mice injected with NT (top) and CREKA (bottom) micelles with 2.5, 5, 10, 25 molar % of DSPE-PEG(2000)-cy7. Micelles with 25 molar % DSPE-PEG(2000)-cy7 (right) clearly show high accumulation in the bladder. (**B**) Cy7 fluorescence of urine samples. No statistical differences were found between samples with the same molar % of cy7.

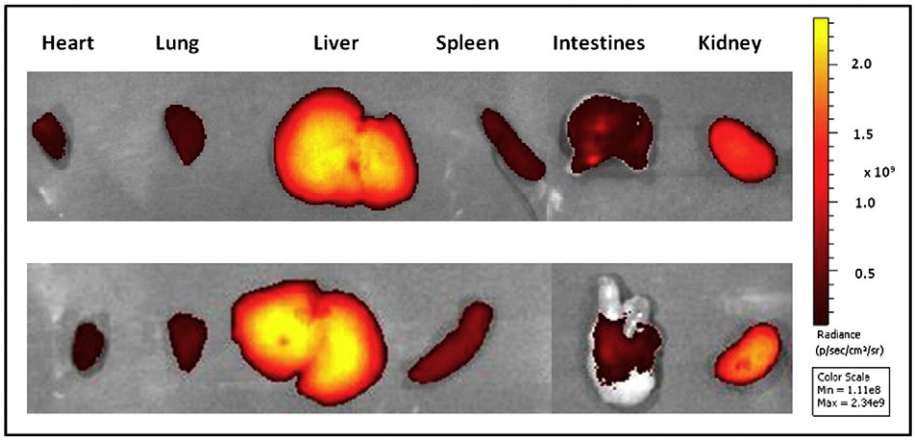

Figure 3. Biodistribution of micelles after 24 h in ApoE knock-out mice. Both NT (top) and CREKA (bottom) micelles accumulated in the liver and kidney.

micelles accumulated in the kidney as well as the lungs. Overall, NT micelles cleared out of the body faster than CREKA micelles at a concentration of 10 mM as shown by the decrease in radiance across all organs after 24 h.

Liver and spleen function

In order to evaluate the potential cytotoxic effects of micelles on the two major organs involved in RES, the liver

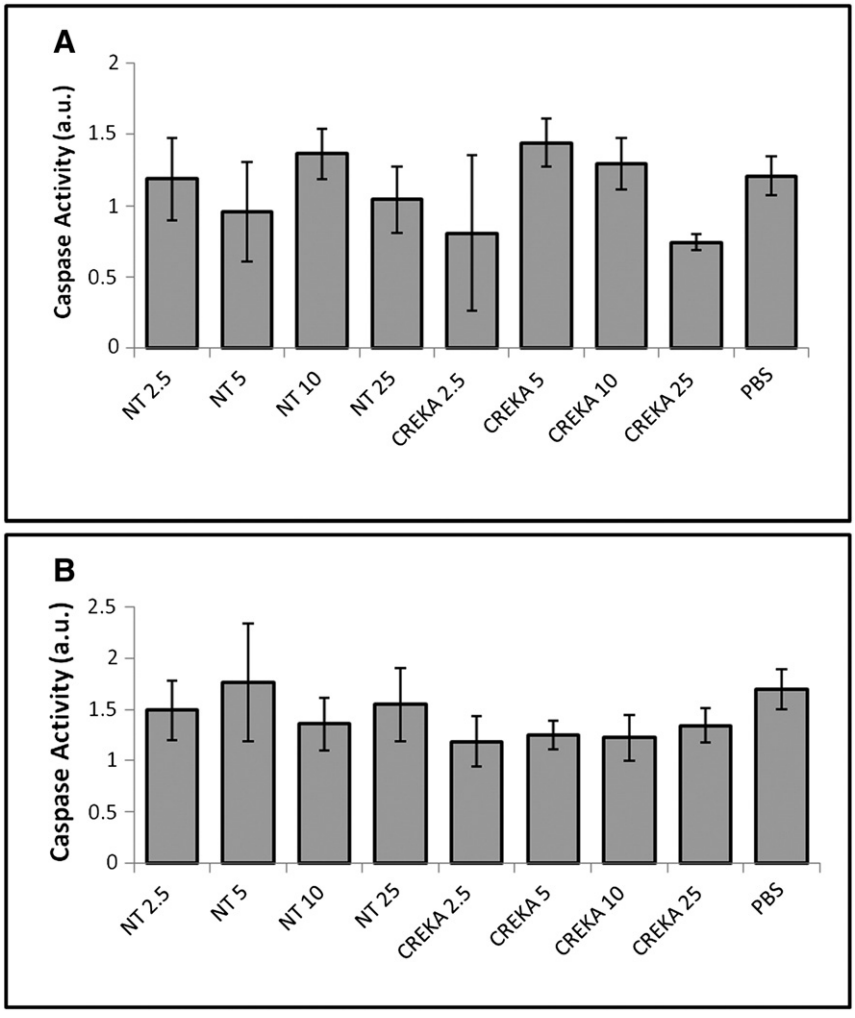

Figure 4. Cytotoxicity of micelles in the liver and the spleen. NT and CREKA micelles did not elicit apoptosis in the (**A**) liver and (**B**) spleen in comparison to PBS-treated groups in ApoE knock-out mice and no statistical differences were found.

and spleen from ApoE knock-out mice treated with NT or CREKA micelles with 2.5, 5, 10, or 25 molar % of DSPE-PEG(2000)-cy7 for 24 h were homogenized and activity of the apoptosis marker, caspase-3, was measured (Figure 4). Both the liver and spleen had levels of caspase activity that were comparable to those of PBS-injected control animals and no statistical significance was found.

To assess liver function, liver tissue levels of alanine aminotransferase (ALT) and asparatate aminotransferase (AST) were measured (Figure 5). For both biochemical parameters and all samples, no statistical differences were found in comparison to the PBS control.

Histological evaluation

Tissue damage of the heart, lung, liver, spleen, intestines, kidney, and bladder upon micelle administration was evaluated through histology. All tissues were stained with hematoxylin and eosin (H&E), examined using light microscopy, and representative images from mice treated with PBS, NT micelles, or CREKA micelle are presented. As seen in Figure 6, no apparent tissue or cellular damage was observed in the ApoE knock-out mice injected with the NT or CREKA micelles when compared to images obtained from mice injected with PBS or WT mice treated with NT or CREKA micelles after 24 h (Supplementary Figure 7), and no pathological changes were observed. No tissue or cellular damage was found in organs derived from mice treated with 10 mM NT or CREKA micelles as well (Supplementary Figure 8).

Discussion

Peptide amphiphiles possess enormous potential as biomaterials for applications in medicine and hold promise as multimodal agents with targeting, regenerative, imaging, and therapeutic capabilities.[12,38,39] Previous work in our laboratory has demonstrated several examples of PAs with clinical relevance, including systems for vaccines,[40,41] cancer,[33,42] and atherosclerosis theranostics.[1] Moreover, other groups report on the utility of PAs as matrices for regenerating tissue including nerves,[43] cartilage,[13] bone,[44] and enamel.[45] Although nanomaterials consisting of PAs have exciting implications for medicine

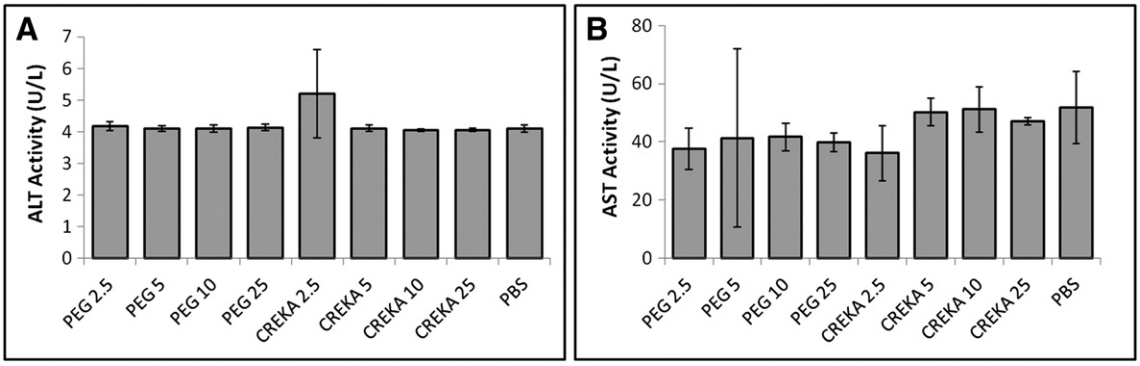

Figure 5. Liver function was assessed by measuring tissue ALT and AST. No statistical differences were found in comparison to PBS-treated groups in ApoE knock-out mice for both assays.

and have been investigated for a variety of clinical needs, studies regarding the *in vivo* behavior and biocompatibility are limited.[46] In this study, we intravenously administered cy7-labeled spherical PA micelles in an atherosclerosis murine model and examined clearance, biodistribution, and toxicity after 24 h.

A variety of studies have previously reported on the dependence of charge and size on the biodistribution and clearance mechanisms of nanoparticles.[24,28,47] The size of both NT and CREKA micelles was determined to be similar (7.8 vs 7.9 nm, Figure 1, Table 1). However, the overall surface charge of NT micelles was found to be negative with an absolute zeta potential value of −22.5 mV, while the CREKA micelles were positively-charged with a zeta potential of 36.3 mV (Table 1). The negative surface charge of NT micelles can be attributed to the phosphate group of the DSPE tail, PEG molecules, and the maleimide. By the addition of the arginine and lysine-containing peptide, the surface charge was reversed.

Despite the difference in surface charge, neither micelle caused red blood cell lysis or aggregation, confirming biocompatibility *in vitro* (Supplementary Figure 1). While cationic particles have been reported to impart hemolytic properties and cause erythrocyte aggregation, our micelle design incorporates PEG which enhances particle half-life in circulation as well as reduces erythrocyte damage.[48] Furthermore, both types of micelles were cleared from the blood primarily through the bladder after 24 h suggesting size to play a larger role in clearance than surface charge in this system (Figure 2, *A*). In addition, fluorescence intensity of urine samples increased linearly with increasing cy7 content further confirming renal clearance of micelles (Figure 2, *B*), a desirable pathway for micelle removal with minimal side effects.[18,21]

Glomerular filtration, or filtration of blood by the kidneys, is the first step of renal clearance and is known to be highly size-selective.[31] Since our micelles are approximately 8 nm in diameter, they fall in the range of molecules that may be capable of both glomerular filtration and renal clearance, and elimination by macrophages in the spleen and liver by RES (also called mononuclear phagocytic system, MPS).[18,21] In addition, it is possible that upon reaching the targeting site, only some amphiphile monomers bind, in turn causing micelle disassembly and clearance of non-bound monomers through the bladder. In addition, although the physical properties of nanoparticles, such as size, can be highly controlled, electrostatic interactions with serum proteins and components, as well as protein adsorption and opsonization processes in the *in vivo* environment are likely to increase the hydrodynamic diameter of both negatively- and positively-charged nanoparticles, which may also contribute to clearance of NT and CREKA micelles via RES.[21,49,50] When NT or CREKA micelles were incubated in cell culture media supplemented with FBS at 37 °C, the diameters of both micelles increased to 9.2 ± 0.4 and 9.5 ± 1.1 nm, respectively (Table S1). Upon *ex vivo* imaging of organs, renal clearance of micelles was further supported by increased fluorescence of the kidneys, although both NT and CREKA micelles were also found to have accumulated substantially within the liver, supporting elimination by RES as well (Figure 3). This was the case in WT mice treated with NT and CREKA micelles as well as ApoE mice treated with micelles at a higher dose (Supplementary Figures 3, 4, 5, and 6). These results are consistent with our recent findings regarding NT and CREKA micelles within a murine, glioblastoma model.[33] By day 7, over 90% of micelles were found to be cleared out of the body (Supplementary Figures 3 and 4).[33]

Caspase-3 activity of the spleen and liver (Figure 4) was comparable to PBS-treated, control mice, and biochemical parameters for liver function were normal (Figure 5). Furthermore, H&E images confirmed the heart, lung, liver, spleen, intestine, kidney, and bladder to show no sign of tissue damage and have morphologies that were similar to those of PBS treated controls, further establishing the safety of PA micelles (Figure 6, Supplementary Figures 7 and 8).

Taken together, we demonstrate *in vivo* biocompatibility and safety of spherical, PA micelles upon intravenous injection in a murine disease model. Furthermore, we elucidate that clearance of PA micelles is achieved primarily through the renal system and illustrate the safety of using PAs for biomedical applications. Future studies will investigate the *in vivo* response of PAs at longer time points and will fully explore the safety of micelles for a wide range of applications.

Appendix A. Supplementary data

Supplementary data to this article can be found online at http://dx.doi.org/10.1016/j.nano.2014.08.006.

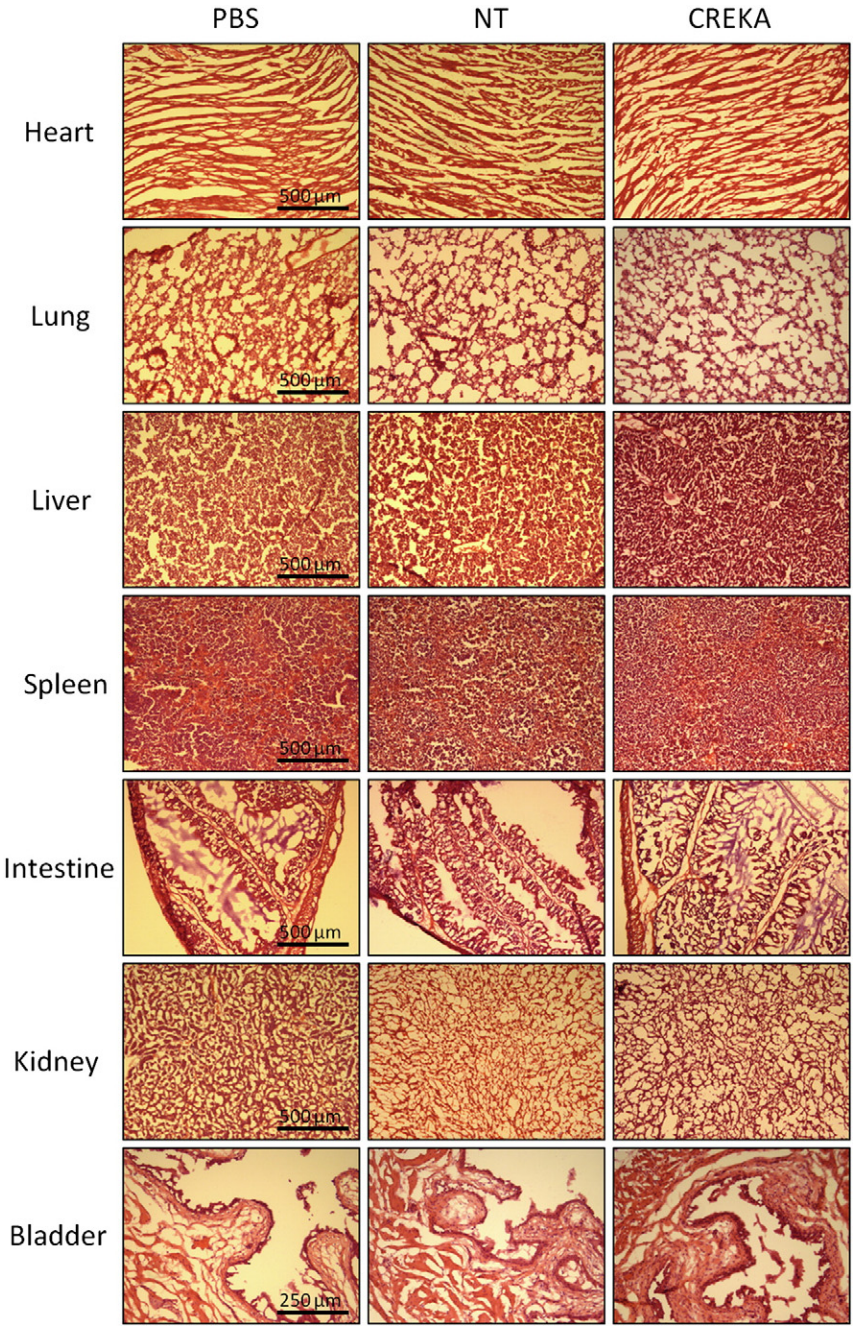

Figure 6. Representative H and E staining of organs treated with NT or CREKA micelles in ApoE knock-out mice shows no morphological changes or tissue damage in comparison to the PBS-treated control.

References

1. Peters D, Kastantin M, Kotamraju VR, Karmali PP, Gujraty K, Tirrell M, et al. Targeting atherosclerosis by using modular, multifunctional micelles. *Proc Natl Acad Sci* 2009;**106**:9815-9.
2. Rosi NL, Giljohann DA, Thaxton CS, Lytton-Jean AKR, Han MS, Mirkin CA. Oligonucleotide-modified gold nanoparticles for intracellular gene regulation. *Science* 2006;**312**:1027-30.
3. Gao XH, Cui YY, Levenson RM, Chung LWK, Nie SM. In vivo cancer targeting and imaging with semiconductor quantum dots. *Nat Biotechnol* 2004;**22**:969-76.
4. Mart RJ, Osborne RD, Stevens MM, Ulijn RV. Peptide-based stimuli-responsive biomaterials. *Soft Matter* 2006;**2**:822-35.
5. Wagh A, Singh J, Qian S, Law B. A short circulating peptide nanofiber as a carrier for tumoral delivery. *Nanomedicine* 2013;**9**:449-57.
6. Hartgerink JD, Beniash E, Stupp SI. Self-assembly and mineralization of peptide-amphiphile nanofibers. *Science* 2001;**294**:1684-8.
7. Tkachenko AG, Xie H, Coleman D, Glomm W, Ryan J, Anderson MF, et al. Multifunctional gold nanoparticle-peptide complexes for nuclear targeting. *J Am Chem Soc* 2003;**125**:4700-1.

8. Zhang SG. Fabrication of novel biomaterials through molecular self-assembly. *Nat Biotechnol* 2003;**21**:1171-8.
9. Akerman ME, Chan WCW, Laakkonen P, Bhatia SN, Ruoslahti E. Nanocrystal targeting in vivo. *Proc Natl Acad Sci U S A* 2002;**99**:12617-21.
10. Cui HG, Webber MJ, Stupp SI. Self-assembly of peptide amphiphiles: from molecules to nanostructures to biomaterials. *Biopolymers* 2010;**94**:1-18.
11. Trent A, Marullo R, Lin B, Black M, Tirrell M. Structural properties of soluble peptide amphiphile micelles. *Soft Matter* 2011;**7**:9572-82.
12. Karmali PP, Kotamraju VR, Kastantin M, Black M, Missirlis D, Tirrell M, et al. Targeting of albumin-embedded paclitaxel nanoparticles to tumors. *Nanomedicine* 2009;**5**:73-82.
13. Shah RN, Shah NA, Del Rosario Lim MM, Hsieh C, Nuber G, Stupp SI. Supramolecular design of self-assembling nanofibers for cartilage regeneration. *Proc Natl Acad Sci* 2010;**107**:3293-8.
14. Peer D, Karp JM, Hong S, FaroKhzad OC, Margalit R, Langer R. Nanocarriers as an emerging platform for cancer therapy. *Nat Nanotechnol* 2007;**2**:751-60.
15. Northfelt DW, Dezube BJ, Thommes JA, Miller BJ, Fischl MA, Friedman-Kien A, et al. Pegylated-liposomal doxorubicin versus doxorubicin, bleomycin, and vincristine in the treatment of AIDS-related Kaposi's sarcoma: results of a randomized phase III clinical trial. *J Clin Oncol* 1998;**16**:2445-51.
16. Gradishar WJ, Tjulandin S, Davidson N, Shaw H, Desai N, Bhar P, et al. Phase III trial of nanoparticle albumin-bound paclitaxel compared with polyethylated castor oil-based paclitaxel in women with breast cancer. *J Clin Oncol* 2005;**23**:7794-803.
17. James ND, Coker RJ, Tomlinson D, Harris JRW, Gompels M, Pinching AJ, et al. Liposomal doxorubicin (Doxil): an effective new treatment for Kaposi's sarcoma in AIDS. *Clin Oncol* 1994;**6**:294-6.
18. Choi HS, Liu W, Misra P, Tanaka E, Zimmer JP, Ipe BI, et al. Renal clearance of quantum dots. *Nat Biotechnol* 2007;**25**:1165-70.
19. Burns AA, Vider J, Ow H, Herz E, Penate-Medina O, Baumgart M, et al. Fluorescent silica nanoparticles with efficient urinary excretion for nanomedicine. *Nano Lett* 2008;**9**:442-8.
20. Li S-D, Huang L. Pharmacokinetics and biodistribution of nanoparticles. *Mol Pharm* 2008;**5**:496-504.
21. Longmire M, Choyke PL, Kobayashi H. Clearance properties of nano-sized particles and molecules as imaging agents: considerations and caveats. *Nanomedicine* 2008;**3**:703-17.
22. Champion JA, Walker A, Mitragotri S. Role of particle size in phagocytosis of polymeric microspheres. *Pharm Res* 2008;**25**:1815-21.
23. Vonarbourg A, Passirani C, Saulnier P, Benoit J-P. Parameters influencing the stealthiness of colloidal drug delivery systems. *Biomaterials* 2006;**27**:4356-73.
24. Duan X, Li Y. Physicochemical characteristics of nanoparticles affect circulation, biodistribution, cellular internalization, and trafficking. *Small* 2013;**9**:1521-32.
25. Rigotti A, Acton SL, Krieger M. The class B scavenger receptors SR-BI and CD36 are receptors for anionic phospholipids. *J Biol Chem* 1995;**270**:16221-4.
26. Roser M, Fischer D, Kissel T. Surface-modified biodegradable albumin nano- and microspheres. II: Effect of surface charges on in vitro phagocytosis and biodistribution in rats. *Eur J Pharm Biopharm* 1998;**46**:255-63.
27. Champion JA, Katare YK, Mitragotri S. Particle shape: a new design parameter for micro- and nanoscale drug delivery carriers. *J Control Release* 2007;**121**:3-9.
28. Arnida, Janát-Amsbury MM, Ray A, Peterson CM, Ghandehari H. Geometry and surface characteristics of gold nanoparticles influence their biodistribution and uptake by macrophages. *Eur J Pharm Biopharm* 2011;**77**:417-23.
29. Piao MJ, Kang KA, Lee IK, Kim HS, Kim S, Choi JY, et al. Silver nanoparticles induce oxidative cell damage in human liver cells through inhibition of reduced glutathione and induction of mitochondria-involved apoptosis. *Toxicol Lett* 2011;**201**:92-100.
30. Chen Y-S, Hung Y-C, Liau I, Huang GS. Assessment of the in vivo toxicity of gold nanoparticles. *Nanoscale Res Lett* 2009;**4**:858-64.
31. Deen WM, Lazzara MJ, Myers BD. Structural determinants of glomerular permeability. *Am J Physiol Ren Physiol* 2001;**281**:F579-96.
32. Kobayashi H, Ogawa M, Alford R, Choyke PL, Urano Y. New strategies for fluorescent probe design in medical diagnostic imaging. *Chem Rev* 2009;**110**:2620-40.
33. Chung, EJ; Cheng, Y; Morshed, R; Nord, K; Han, Y; Wegscheid, ML, et al. Fibrin-binding, peptide amphiphile micelles for targeting glioblastoma *Biomaterials 35, 2014, 1249–1256.*
34. Chattopadhyay A, London E. Fluorimetric determination of critical micelle concentration avoiding interference from detergent charge. *Anal Biochem* 1984;**139**:408-12.
35. Rotstein R, Landau T, Twig A, Rubinstein A, Koffler M, Justo D, et al. The erythrocyte adhesiveness/aggregation test (EAAT): a new biomarker to reveal the presence of low grade subclinical smoldering inflammation in individuals with atherosclerotic risk factors. *Atherosclerosis* 2002;**165**:343-51.
36. Whitman SC. A practical approach to using mice in atherosclerosis research. *Clin Biochem Rev Aust Assoc Clin Biochem* 2004;**25**:81-93.
37. Ashok B, Arleth L, Hjelm RP, Rubinstein I, Önyüksel H. In vitro characterization of PEGylated phospholipid micelles for improved drug solubilization: effects of PEG chain length and PC incorporation. *J Pharm Sci* 2004;**93**:2476-87.
38. Lin BF, Megley KA, Viswanathan N, Krogstad DV, Drews LB, Kade MJ, et al. pH-responsive branched peptide amphiphile hydrogel designed for applications in regenerative medicine with potential as injectable tissue scaffolds. *J Mater Chem* 2012;**22**:19447-54.
39. Mlinar LB, Chung EJ, Wonder EA, Tirrell M. Active targeting of early and mid-stage atherosclerotic plaques using self-assembled peptide amphiphile micelles. *Biomaterials* 2014;**35**:8678-86.
40. Mitchell D, Yong M, Raju J, Willemsen N, Black M, Trent A, et al. Toll-like receptor-mediated adjuvanticity and immunomodulation in dendritic cells: implications for peptide vaccines. *Hum Vaccin* 2011;**7**:85-93.
41. Black M, Trent A, Kostenko Y, Lee JS, Olive C, Tirrell M. Self-assembled peptide amphiphile micelles containing a cytotoxic T-cell epitope promote a protective immune response in vivo. *Adv Mater* 2012;**24**:3845-9.
42. Missirlis D, Khant H, Tirrell M. Mechanisms of peptide amphiphile internalization by SJSA-1 cells in vitro. *Biochemistry* 2009;**48**:3304-14.
43. Angeloni NL, Bond CW, Tang Y, Harrington DA, Zhang S, Stupp SI, et al. Regeneration of the cavernous nerve by Sonic hedgehog using aligned peptide amphiphile nanofibers. *Biomaterials* 2011;**32**:1091-101.
44. Hosseinkhani H, Hosseinkhani M, Tian F, Kobayashi H, Tabata Y. Ectopic bone formation in collagen sponge self-assembled peptide-amphiphile nanofibers hybrid scaffold in a perfusion culture bioreactor. *Biomaterials* 2006;**27**:5089-98.
45. Huang Z, Newcomb CJ, Zhou Y, Lei YP, Bringas Jr P, Stupp SI, et al. The role of bioactive nanofibers in enamel regeneration mediated through integrin signals acting upon C/EBPα and c-Jun. *Biomaterials* 2013;**34**:3303-14.
46. Fischer HC, Chan WCW. Nanotoxicity: the growing need for in vivo study. *Curr Opin Biotechnol* 2007;**18**:565-71.
47. Sonavane G, Tomoda K, Makino K. Biodistribution of colloidal gold nanoparticles after intravenous administration: effect of particle size. *Colloids Surf B: Biointerfaces* 2008;**66**:274-80.
48. Dobrovolskaia MA, Aggarwal P, Hall JB, McNeil SE. Preclinical studies to understand nanoparticle interaction with the immune system and its potential effects on nanoparticle biodistribution. *Mol Pharm* 2008;**5**:487-95.
49. Yu SS, Lau CM, Thomas SN, Jerome WG, Maron DJ, Dickerson JH, et al. Size- and charge-dependent non-specific uptake of PEGylated nanoparticles by macrophages. *Int J Nanomedicine* 2012;**7**:799-813.
50. Mortensen NP, Hurst GB, Wang W, Foster CM, Nallathamby PD, Retterer ST. Dynamic development of the protein corona on silica nanoparticles: composition and role in toxicity. *Nanoscale* 2013;**5**:6372-80.